Polymer Degradation and Stability 97 (2012) 108–117

Contents lists available at SciVerse ScienceDirect

Polymer Degradation and Stability

journal homepage: www.elsevier.com/locate/polydegstab

Effects of organoclay modifiers on the flammability, thermal and mechanical properties of polycarbonate nanocomposites filled with a phosphate and organoclays

Jie Feng, Jianwei Hao*, Jianxin Du, Rongjie Yang

National Laboratory of Flame Retardant Materials, School of Materials Science and Engineering, Beijing Institute of Technology, 5 South Zhongguancun Street, Haidian District, Beijing 100081, PR China

ARTICLE INFO

Article history:
Received 28 August 2011
Accepted 28 September 2011
Available online 5 October 2011

Keywords:
Polycarbonate nanocomposites
Flame retardancy
Thermal degradation
Glass transition temperature
Mechanical properties

ABSTRACT

Polycarbonate was melt blended with solid bisphenol A bis(diphenyl phosphate), and a series of organoclays. Effects of the organoclay modifiers on the flammability, thermal and mechanical properties of the nanocomposites were studied by limiting oxygen index, UL-94 burning test, thermogravimetric analysis, differential scanning calorimetry, tensile test and dynamic mechanical analysis. Although all the nanocomposites exhibit an intercalated-exfoliated morphology, they vary in the magnitude of intercalation revealed by X-ray diffraction and transmission electron microscopy. Flammability of the nanocomposites is strongly related to the thermal stability rather than the morphology. Glass transition temperature (T_g) and mechanical properties are controlled by both the morphology and the affinity of the organoclays with the matrix. The modifier containing hydroxyl moiety has stronger interactions with the matrix but it can promote its degradation, thus the corresponding nanocomposite exhibits a better intercalated morphology, higher T_g, superior strength and modulus however a worse thermal stability and flame retardancy. An additional silane within the organoclays would make the organoclays more compatible with the matrix but be a steric obstacle to the intercalation of the matrix chains; however, flame retardancy of the corresponding nanocomposite is enhanced due to the flame retardant nature of the silane. Similarly, the modifier bearing two long alkyl tails shows stronger affinity with the matrix than the one bearing a single tail, but it would hinder the intercalation due to the steric effect. These establishments between organoclay modifiers and the properties of nanocomposites might be guidance for developing materials with practical applications.

1. Introduction

As an engineering thermoplastic, bisphenol A polycarbonate (PC) has been widely used in the fields of transport, construction, packaging, optics, electrics and electronics owing to its excellent mechanical properties, insulation, high heat distortion temperature and extraordinary transparency. Although PC is less flammable than many polyolefins or polyesters, fire hazard is still serious especially under some critical applications.

Representative flame retardants used in PC include halogenated and halogen-free compounds. Since halogenated compounds are gradually banned due to environmental concerns, halogen-free compounds such as phosphorus containing, sulfur containing and siloxane compounds are quite promising [1,2]. Among the phosphorus containing compounds, bisphenol A bis(diphenyl phosphate) (BDP) is a rather important one for its high hydrolytic resistance, thermal stability, low volatility and good compatibility with PC. The flame retardancy mechanism of BDP is mainly explained by the promotion of the char residue formation in the condensed phase. However, BDP would exhibit some plasticizing effects therefore induce the glass transition temperature (T_g) and heat distortion temperature of the matrix to decrease [3]. In order to overcome the drawback of BDP, we chose the polymer–clay nanocomposites technology.

Since the successful application of nylon 6-clay nanocomposites in automobiles [4–6], polymer–clay nanocomposites technology has motivated vigorous researches from both academia and industry. Due to the extremely large surface areas and high aspect ratios of the nanoclays, multiple properties of the matrices such as mechanical, thermal and barrier properties could be prominently

* Corresponding author. Tel./fax: +86 10 68913075.
E-mail address: hjw@bit.edu.cn (J. Hao).

0141-3910/$ – see front matter © 2011 Elsevier Ltd. All rights reserved.
doi:10.1016/j.polymdegradstab.2011.09.019

improved with only small filler loadings [7–12]. Almost all the nanocomposites could result in a significant enhancement of modulus to be much stiffer, which is rather desirable for engineering applications. Nylon 6 with an increased heat distortion temperature of nearly 90 °C was reported [6]. However, the variations of T_g are indefinite. Compared with neat polymers, both increased [13], degreased [14] and even absent or an extremely weak T_g [15] were found within different nanocomposites.

Many attempts have been devoted to prepare PC–clay nanocomposites [16–27]. People used different preparation methods and also a series of clays exchanged with various surfactants to study one or multiple properties of the PC nanocomposites; however, an integrated understanding of how the organoclay modifiers could affect the thermal and mechanical properties of PC nanocomposites is not yet entirely established. Most morphologies of the clays in the nanocomposites were intercalated, whereas exfoliated morphologies were achieved via methodologies such as ring-opening polymerization of cyclic oligomers [16] or in situ melt polycondensation [27]. Yoon et al. prepared PC–clay nanocomposites via melt extrusion and the moduli of the nanocomposites varied with the structures of the clay modifiers [19]. Hsieh et al. found a depression of T_g with the increasing loading of clays [20], while a constant T_g was found by Chow et al. [23]; these two results were obtained from dynamic mechanical analysis (DMA). However, Lee et al. detected an increased T_g by using differential scanning calorimetry (DSC) [17] and Nayak et al. also observed an enhanced T_g by using both DMA and DSC [26].

In our previous work, we have incorporated the solid BDP (S-BDP) and one type of organoclay (montmorillonite-based) into PC by twin-screw extrusion [28]. The resulting nanocomposite exhibited mainly intercalated and partially exfoliated morphology. A synergistic effect on flame retardancy could be found in the UL-94 vertical burning test. The flame retardancy mechanism of the nanocomposite was explained by the improved thermal oxidative stability of the char residue. S-BDP would also contribute some flame inhibition effects in the gaseous phase, especially filling alone in the matrix. When added in the nanocomposite, gaseous phase effects of S-BDP would be weakened thereby condensed phase effects would be enhanced under the presence of organoclays [29]. S-BDP is preferable because of its conveniences during transport and manufacture compared to the conventional sticky liquid BDP; however, the drawback of BDP mentioned above remains unchanged.

In this article, we focus on the flammability, mechanical and thermal properties of PC nanocomposites filled with the S-BDP and organoclays. Four types of organoclays with different organic modifiers were applied. Flammability, morphology, thermal stability, T_g and mechanical properties of the nanocomposites were elaborately examined. This research may not only understand the effects of the clay modifiers on these above properties of the nanocomposites, but also introduce a flame retarded PC with potential practical applications.

2. Experimental

2.1. Materials

Bisphenol A polycarbonate (Makrolon 2805) was purchased from Bayer (Shanghai), solid bisphenol A bis(diphenyl phosphate) (S-BDP) was provided by Yoke Chemical Co., Ltd. and polytetrafluoroethylene (PTFE) was obtained from Songbai Chemicals Company. Four types of organoclays used herein were Nanomer I.34TCN, I.44P, I.44PS and I.31PS from Nanocor Inc. These organoclays were montmorillonites modified by a cation-exchanged procedure with different kinds of quaternary ammonium surfactants; besides, I.44PS and I.31PS were additionally treated with a silane coupling agent. The structures of modifiers used for each organoclay are illustrated in Fig. 1. PC, PTFE and organoclays were dried for 12 h at 100 °C prior to process, whereas the S-BDP was used as received.

2.2. Sample preparation

Dehumidified PC was melt blended with the above addictives using a co-rotating twin-screw extruder (SHJ-20, Nanjing Giant Machinery Co., Ltd.) with a rotary speed of 200 rpm and a screw temperature profile of 235, 240, 245, 250, 242, 232 °C from the hopper to the die. Extrudate was cooled with water bath and pelletized subsequently. Specimens with various shapes, corresponding to the characterizations discussed below, were formed using an injection-moulding machine (HTF90X1, Haitian Plastic Machinery Ltd.) operated at an injection temperature profile of 250, 256, 263, 270, 265 °C.

2.3. Characterization

Flammability of the samples was evaluated by limiting oxygen index (LOI) and UL-94 vertical burning test. The LOI value was measured on an FTA-II instrument (Rheometric Scientific Ltd.) with a specimen dimension of 130 × 6.5 × 3 mm^3, according to the ASTM D 2863-08 standard. The UL-94 vertical burning test was carried out with a CZF-3 instrument (Jiangning Analysis Instrument Factory) with a specimen dimension of 125 × 12.5 × 3.2 mm^3.

X-ray diffraction (XRD) data were collected on an X′ Pert PRO MRD diffractometer (PANalytical) using Cu Kα radiation (λ = 0.154 nm). For transmission electron microscopy (TEM), the sample was cryo-microtomed with a glass knife on a Leica ultracut UCT microtome, to give sections with a nominal thickness of 50 nm. The sections were transferred to 200-mesh copper grids. Bright field TEM images were obtained on a Hitachi H-800 at an accelerating voltage of 200 kV.

Thermogravimetric analysis (TGA) was performed on a Netzsch TG 209 F1 apparatus to investigate the thermal decomposition of the samples under a N_2 flow. Samples weighting 5 mg were heated from 40 °C up to 800 °C with a heating rate of 10 °C/min.

Differential scanning calorimetry (DSC) was conducted on a Netzsch DSC 204 F1 instrument. The samples were first heated to

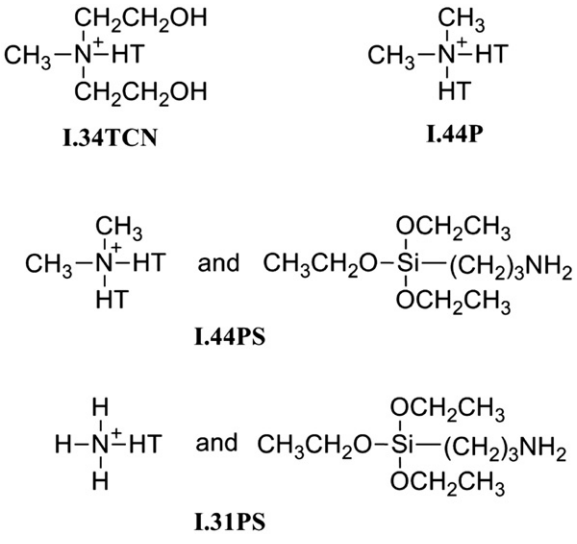

Fig. 1. Chemical structures of the modifiers used for each organoclay, where HT refers to hydrogenated tallow.

200 °C, then cooled to 25 °C, and finally heated to 200 °C. The heating and cooling rates for all runs were 10 °C/min and results within the second heating program are reported.

Tensile tests were carried out on a universal testing machine (DXLL-5000, Shanghai D&G Machinery Equipment Co., Ltd.) according to ASTM D 638-08. Dumbbell shaped specimens were clamped, and an extensometer with a 50 mm gauge length was used to determine the modulus and strength. The rate of crosshead motion was 50 mm/min. Data of 5 tests bars were collected. Dynamic mechanical analysis (DMA) was performed on a Mettler Toledo DMA/SDTA861e instrument using a shear mode. The specimen with a dimension of 5 × 5 × 1.6 mm^3 was heated from 25 to 180 °C at a rate of 3 °C/min. Storage modulus (G'), loss modulus (G'') and loss factor (tan δ) were simultaneously acquired at a frequency of 1 Hz.

3. Results

3.1. Flammability

Compositions of the polycarbonate nanocomposites as well as their LOI and UL-94 tests results are summarized in Table 1.

In order to rule out the influence of processing on the properties of the materials discussed in this research, neat PC was also firstly melt extruded and then injection moulded rather than directly injection moulded with the pellets as received.

From Table 1, it can be seen that neat PC has a LOI value of 25.3% and rates V-2 in the UL-94 burning test because of the dripping. With 6 wt. % of S-BDP and 0.4 wt. % PTFE, the LOI value increases to 28.6% and the dripping is suppressed; however the rating only reaches V-1. Increasing the loading of S-BDP to be 8 wt. %, the LOI value further elevates to 29.4% and a V-0 rating is finally achieved. PC filled with 6 wt. % of S-BDP and 0.4 wt. % PTFE is abbreviated as "PC/S-BDP" hence.

Regarding the nanocomposites, samples of each organoclay series exhibit somewhat alike trends in the LOI values and UL-94 test results. Whichever type of the organoclay used, the worst case is always PC filled with 8 wt. % organoclay and 0.4 wt. % PTFE, even worse than neat PC; the highest LOI value and the best UL-94 test result is obtained by adding 2 wt. % organoclay, 6 wt. % S-BDP and 0.4 wt. % PTFE. For I.44P, I.44PS and I.31PS, samples filled with the combination of 2 wt. % organoclay, 6 wt. % S-BDP and 0.4 wt. % PTFE exhibit a lower LOI value but a shorter after-flame time compared with PC filled with 8 wt. % of S-BDP and 0.4 wt. % PTFE. This phenomenon is explained by the different burning condition between LOI and UL-94 tests [28]. The following characterizations are focused on PC filled with 2 wt. % organoclay, 6 wt. % of S-BDP and 0.4 wt. % PTFE, and the samples are abbreviated as "PC/S-BDP/(organoclay type)" hence (*e.g.*, PC/S-BDP/I.34TCN refers to the sample containing 2 wt. % I.34TCN, 6 wt. % of S-BDP and 0.4 wt. % PTFE).

Among the four types of organoclay, PC/S-BDP/I.34TCN exhibits the lowest LOI value and only achieves a V-1 rating in the UL-94 test; whereas PC/S-BDP/I.44PS shows the best behaviour of flame retardancy in both the LOI value and UL-94 test. The difference of flammability between PC/S-BDP/I.44P and PC/S-BDP/I.31PS is subtle.

3.2. Sample morphology

The morphology of the different types of organoclays in the nanocomposites was examined by XRD and TEM.

XRD patterns of each organoclay and its corresponding nanocomposite are shown in Fig. 2. All nanocomposites exhibit an unambiguous peak of 001 plane at a smaller angle compared with their corresponding unfilled organoclays, suggesting clays are intercalated in the nanocomposites. Calculated by Bragg equation, the d_{001} spacings for each organoclay and corresponding nanocomposite are listed in Table 2. The change of d_{001} spacing (Δd) is calculated by subtracting d_{001} spacing of the organoclay from its corresponding nanocomposite. The increment of d_{001} spacing in the nanocomposite containing I.31PS or I.34TCN is higher than that in the nanocomposite containing I.44P or I.44PS, indicating a better dispersion occurs in the I.31PS or I.34TCN containing sample.

TEM images of the nanocomposites are shown in Fig. 3. It can be seen that all organoclays are rather homogeneously distributed at the nanometric lever in the matrix from the low magnification images. The high magnification images clearly reveal that most of the particles are tactoids with multiple aluminosilicate layers while exfoliated clay platelets can be also observed occasionally. Thus, all the four nanocomposites exhibit a mainly intercalated

Table 1
LOI and UL-94 tests results of the polycarbonate nanocomposites.

Series	PC (wt. %)	Organoclay (wt. %)	S-BDP (wt. %)	PTFE (wt. %)	LOI (%)	UL-94 (3.2 mm)[a]			
						Rating	t_1 (s)	t_2 (s)	Dripping
	100	0	0	0	25.3	V-2	15.3	13.0	Yes
	93.6	0	6	0.4	28.6	V-1	7.0	4.2	No
	91.6	0	8	0.4	29.4	V-0	5.3	3.9	No
I.34TCN	91.6	2	6	0.4	26.6	V-1	9.7	8.8	No
	91.6	4	4	0.4	25.8	NR	18.2	19.7	No
	91.6	6	2	0.4	25.1	NR	20.1	18.7	No
	91.6	8	0	0.4	23.2	NR	28.8	25.3	Yes
I.44P	91.6	2	6	0.4	27.6	V-0	4.1	2.2	No
	91.6	4	4	0.4	26.8	V-1	7.8	5.6	No
	91.6	6	2	0.4	26.3	NR	18.4	14.8	No
	91.6	8	0	0.4	23.9	NR	21.2	15.3	No
I.44PS	91.6	2	6	0.4	28.3	V-0	3.5	1.5	No
	91.6	4	4	0.4	27.2	V-1	6.8	4.9	No
	91.6	6	2	0.4	26.4	NR	19.0	13.5	No
	91.6	8	0	0.4	24.0	NR	20.3	16.5	No
I.31PS	91.6	2	6	0.4	27.8	V-0	4.5	1.9	No
	91.6	4	4	0.4	27.0	V-1	7.5	6.1	No
	91.6	6	2	0.4	26.1	NR	18.8	15.3	No
	91.6	8	0	0.4	23.5	NR	23.1	18.5	No

[a] Results are reported as the average value of 5 test bars.

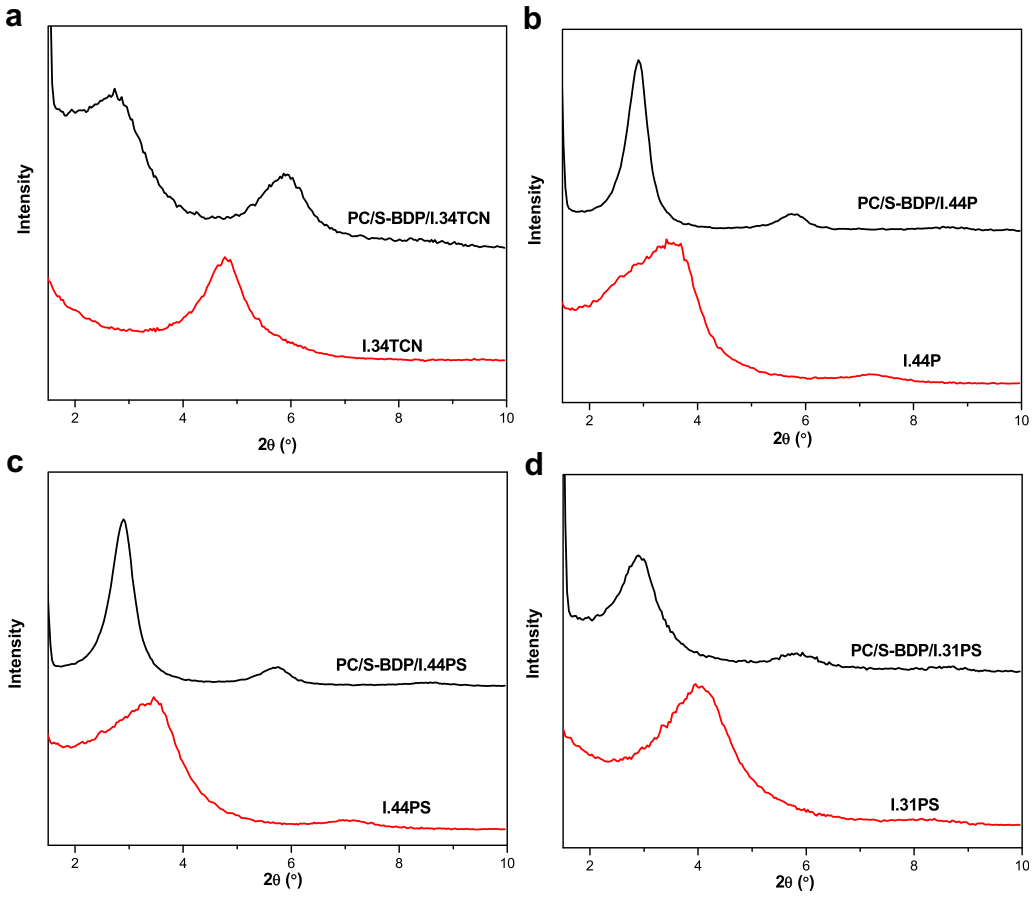

Fig. 2. XRD patterns of (a) I.34TCN, (b) I.44P, (c) I.44PS, (d) I.31PS and their corresponding nanocomposite.

and partially exfoliated morphology. It is also noticed that the clay tactoids in the sample containing I.34TCN (Fig. 3a$_2$) or I.31PS (Fig. 3d$_2$) are more severely swollen and twisted compared with those in the sample containing I.44P (Fig. 3b$_2$) or I.44PS (Fig. 3c$_2$), which is coherent with the result from XRD.

3.3. TGA

Thermal decomposition of the samples under an inert atmosphere was analyzed by TGA, and the results are shown in Figs. 4 and 5 and Table 3.

After adding 6 wt. % S-BDP and 0.4 wt. % PTFE into PC, the material is not thermally as stable as neat PC, showing both a decreased $T_{-5\%}$ and T_{max}; and the amount of char residue at 800 °C remains unchanged compared with neat PC. The situation of organoclay containing samples is quite complicated. Except for PC/S-BDP/I.31PS, samples filled with additional 2 wt. % organoclay exhibit an even lower $T_{-5\%}$ than PC/S-BDP. The quaternary ammonium surfactant used for organic modification of organoclay is relatively unstable. It would undergo the Hoffman elimination at lower temperatures to from an amine and a corresponding olefin, leaving an acidic site on the silicate layer [28,30]. This would be the factor causing the earlier initial decomposition of the nanocomposites. Nevertheless, clay platelets would migrate to the surface of the nanocomposite, displaying an excellent barrier effect to protect the underneath matrix. Thus, T_{max} of all the nanocomposites are elevated than PC/S-BDP, even PC/S-BDP/I.44P shows a higher T_{max} compared with neat PC.

As regards the char residue of the samples at 800 °C, PC/S-BDP exhibits no difference compared to neat PC; however, nanocomposites would leave more char residue than both neat PC and PC/S-BDP except for PC/S-BDP/I.34TCN. More clearly results can be obtained by subtracting the char residue of corresponding organoclay heated alone to 800 °C from the original amount of char residue of the nanocomposites at 800 °C (R_2 column in Table 3). The result shows that the matrix would leave the highest amount of char residue in the presence of I.44PS, whereas the lowest amount of char residue in the presence of I.34TCN.

Table 2
The d_{001} spacing for each organoclay and it corresponding nanocomposite.

Sample	2θ (°)	d_{001} spacing (nm)	Δd (nm)
I.34TCN	4.81	1.84	1.43
PC/S-BDP/I.34TCN	2.70	3.27	
I.44P	3.54	2.49	0.55
PC/S-BDP/I.44P	2.91	3.04	
I.44PS	3.47	2.55	0.50
PC/S-BDP/I.44PS	2.89	3.05	
I.31PS	4.01	2.20	0.85
PC/S-BDP/I.31PS	2.90	3.05	

3.4. DSC

The glass transition behaviour of the samples was investigated by DSC, and the results are shown in Fig. 6 and Table 4.

As expected, all the samples exhibit only a second-order transition in the DSC curves, indicating the glass transition temperature

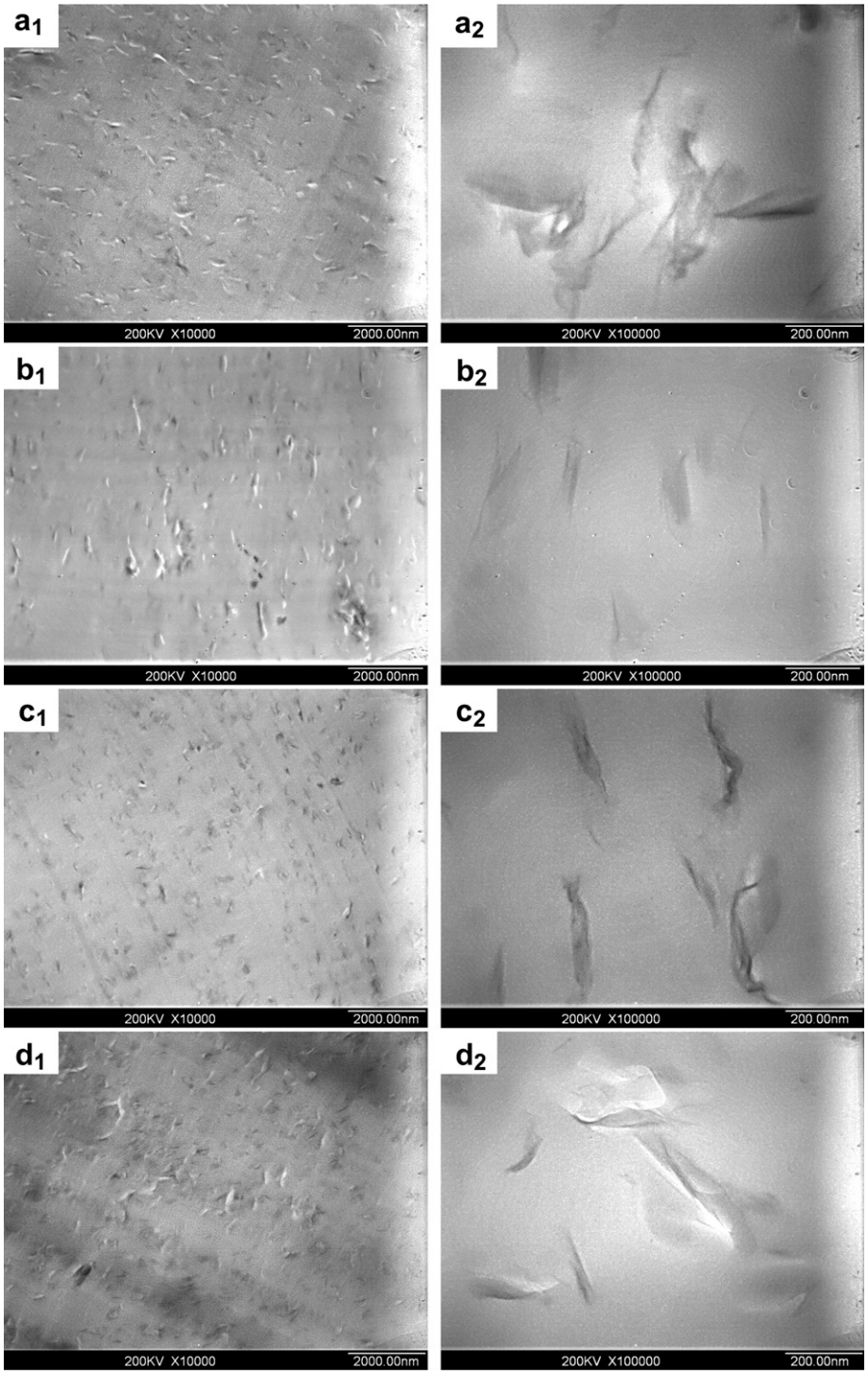

Fig. 3. Low magnification (left column) and high magnification (right column) TEM images of the nanocomposites: (a) PC/S-BDP/I.34TCN, (b) PC/S-BDP/I.44P, (c) PC/S-BDP/I.44PS, (d) PC/S-BDP/I.31PS.

(T_g). Neither neat PC nor any nanocomposite shows a crystallization exothermic peak due to the amorphous instinct of the bisphenol A PC used here.

Neat PC has a high T_g at 143 °C, whereas the T_g of PC/S-BDP decreases dramatically by 24 °C attributing to the plasticizing effect of S-BDP. However, in the case of nanocomposites, there are significant increments in T_g with the 2 wt. % organoclay. Among the four types of organoclay, I.34TCN gives the greatest increase in T_g by 10 °C compared to PC/S-BDP. The order of the T_g of the nanocomposites is PC/S-BDP/I.34TCN > PC/S-BDP/I.44PS > PC/S-BDP/I.31PS > PC/S-BDP/I.44P.

3.5. Mechanical properties

Mechanical properties of the samples were evaluated by tensile tests and DMA. Storage modulus and loss factor spectra from DMA are illustrated in Fig. 7. Detailed data from tensile tests and DMA are listed in Table 5.

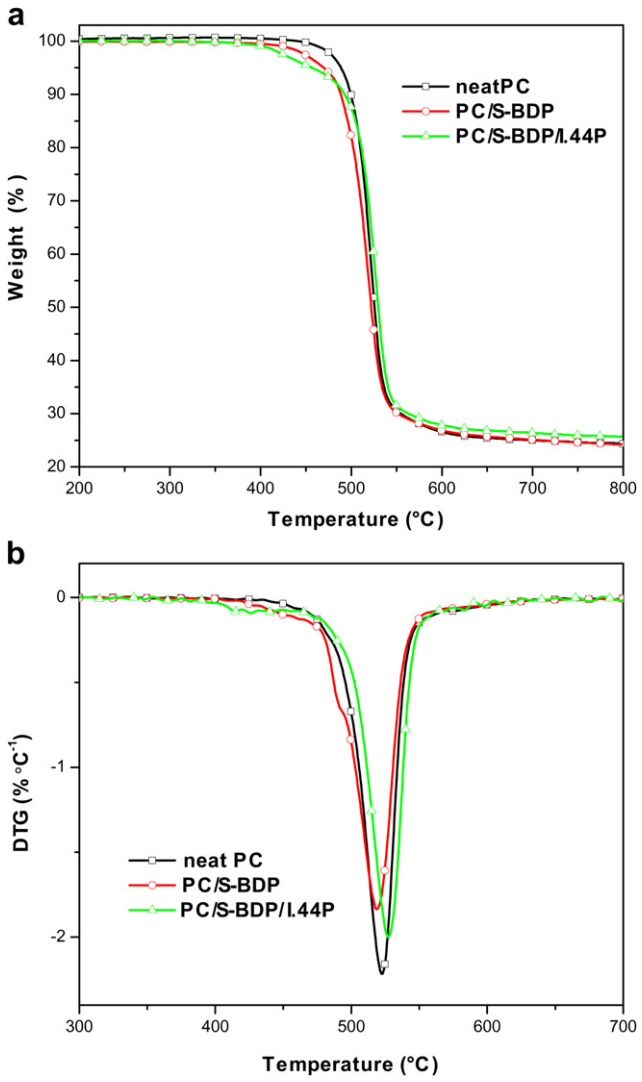

Fig. 4. (a) TGA and corresponding (b) DTG curves of neat PC, PC/S-BDP and PC/S-BDP/I.44P.

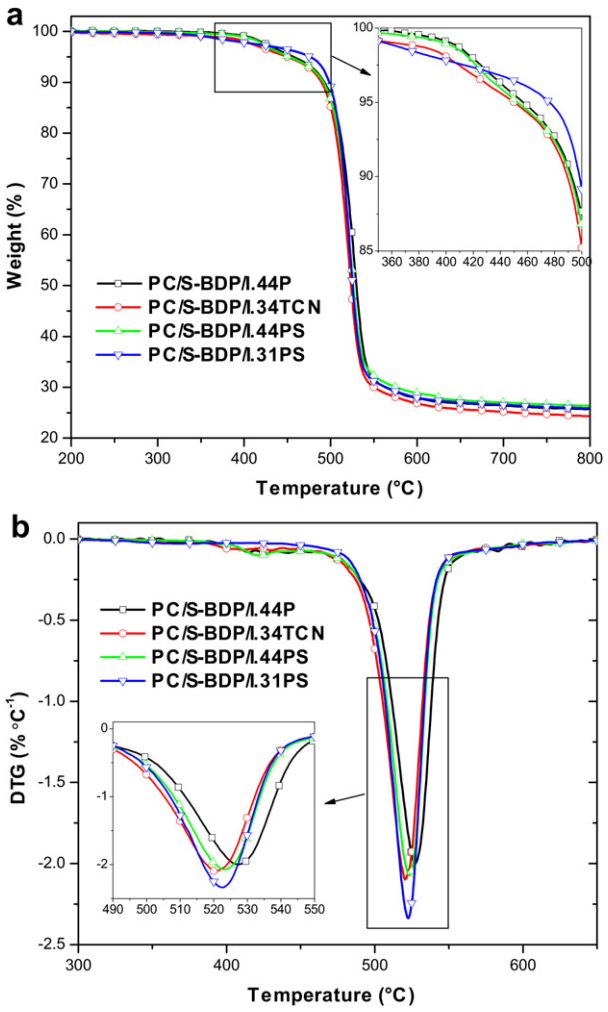

Fig. 5. (a) TGA and corresponding (b) DTG curves of the nanocomposites (the insets are enlarged figures).

The mechanical data of neat PC provided by the supplier [31], which is tensile strength = 66 MPa and tensile modulus = 2400 MPa, are a little higher than those we detected in this research. This may attribute to the slight degradation caused by heat and shear during the extrusion procedure. After adding 6 wt. % S-BDP and 0.4 wt. % PTFE, a marginal increase of tensile strength however a decrease of Young's modulus and elongation at break can be observed. In the case of nanocomposites, both tensile strength and Yong's modulus are prominently increased compared with neat PC and PC/S-BDP. Unfortunately, all the nanocomposites are more brittle showing great depressions in the elongation at break. The order of the tensile strengths of the nanocomposites is PC/S-BDP/I.34TCN > PC/S-BDP/I.31PS > PC/S-BDP/I.44P > PC/S-BDP/I.44PS, and the trend of Young's modulus is the same as tensile strength.

From Fig. 7, it can be found that storage moduli of PC/S-BDP over time are largely reduced, whereas those of the nanocomposites are enhanced compared to neat PC. Specific storage moduli at 30 °C and 100 °C are recorded in Table 5. The changes of G' at 30 °C and 100 °C follow the same trend as Young's modulus from tensile tests. T_g suggested by DMA is estimated by the temperature at the maximum value of tan δ in Fig. 7b. PC/S-BDP exhibits a remarkably decreased T_g as same as the result obtained in DSC. However, the variations among the nanocomposites are not consistent with the results from DSC. This phenomenon was already noticed previously. It is believed that DSC reveals the thermodynamics whereas DMA indicates the thermo-mechanical properties of the polymer, the temperature at the maximum value of tan δ represents an "apparent" thermo-mechanical transition rather than the thermodynamic glass transition. The maximum value of tan δ is more sensitive to parameters such as the filler content or morphology

Table 3
TGA data of the PC nanocomposites.

Sample	$T_{-5\%}$ (°C)[a]	T_{max} (°C)[b]	R_1 (%)[c]	R_2 (%)[d]
Neat PC	489	523	24.4	\
PC/S-BDP	470	519	24.2	\
PC/S-BDP/I.34TCN	450	521	24.3	22.8
PC/S-BDP/I.44P	457	527	25.9	24.6
PC/S-BDP/I.44PS	453	523	26.4	25.2
PC/S-BDP/I.31PS	476	522	25.9	24.5

[a] $T_{-5\%}$: temperature at 5% weight loss.
[b] T_{max}: temperature at the maximum weight loss rate derived from DTG.
[c] R_1: the original amount of char residue of the samples at 800 °C.
[d] R_2: the calculated amount of char residue of the nanocomposites by subtracting the residue of corresponding organoclay heated alone to 800 °C from the original amount of char residue of the nanocomposites at 800 °C.

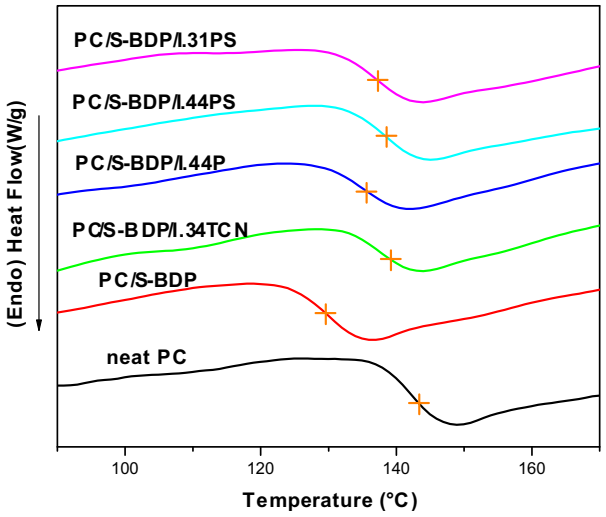

Fig. 6. DSC curves of neat PC, PC/S-BDP and the nanocomposites.

than the glass transition [32,33]. Thus, the results of T_g suggested by DSC are more convincing.

4. Discussion

The main differences of the four types of organoclay employed here lie on the modifiers used in the organic modification of the clays. As illustrated in Fig. 1, the quaternary ammonium of I.34TCN contains a single long alkyl tail as well as two hydroxyl moieties, and the ammonium of I.44P has two long alkyl tails. Compared to I.44P, I.44PS is additionally modified with a silane coupling agent. I.31PS is different from I.44PS because the quaternary ammonium of I.31PS has only one long alkyl tail. The differences of the modifiers may result in the diverse properties of the nanocomposites.

From the XRD results, I.44P and I.44PS, with two long alkyl tails ammoniums, exhibit almost a same increase in d_{001} spacing of approximate 0.5 nm after incorporating into the matrix (Table 2). Aranda and Chen suggested that 0.4 nm is equivalent to a planar zigzag monolayer of poly(ethylene oxide) [34] or poly(ε-caprolactone) [35] molecules. It is assumed that the Δd of 0.5 nm here is caused by a planar monolayer of PC molecular chains intercalated into the galleries of the organoclays. The slight difference of the monolayer thickness between poly(ethylene oxide), poly(ε-caprolactone) and PC could be attributed to the steric effect of the relatively larger aromatic rings in the backbones of PC. As for I.31PS, the ammonium with one long tail exhibits a smaller steric effect compared with the two long tails ammonium in I.44PS, leading to a higher Δd of 0.85 nm. The molecules of PC might intercalate into the clay galleries showing a lateral bilayer or an inclined lay-to-lay configuration [36]. The hydroxyl moieties of the ammonium used in I.34TCN would be inclined to form hydrogen bonds with PC [17], so the affinity between the modifier and the matrix would allow more matrix chains to intercalate into the clay galleries. The highest Δd of 1.43 nm in the I.34TCN containing nanocomposite may correspond to a planar "trilayer" or a folded configuration [36] of PC molecules. Also, it's worthy to note that a higher Δd implies less tightly stacking of clay platelets thereby producing more chances of exfoliation.

Table 4
DSC data of the PC nanocomposites.

Sample	T_g determined by DSC (°C)	ΔC_P at T_g ($Jg^{-1}\,K^{-1}$)
Neat PC	143	0.243
PC/S-BDP	129	0.214
PC/S-BDP/I.34TCN	139	0.175
PC/S-BDP/I.44P	136	0.191
PC/S-BDP/I.44PS	138	0.193
PC/S-BDP/I.31PS	137	0.184

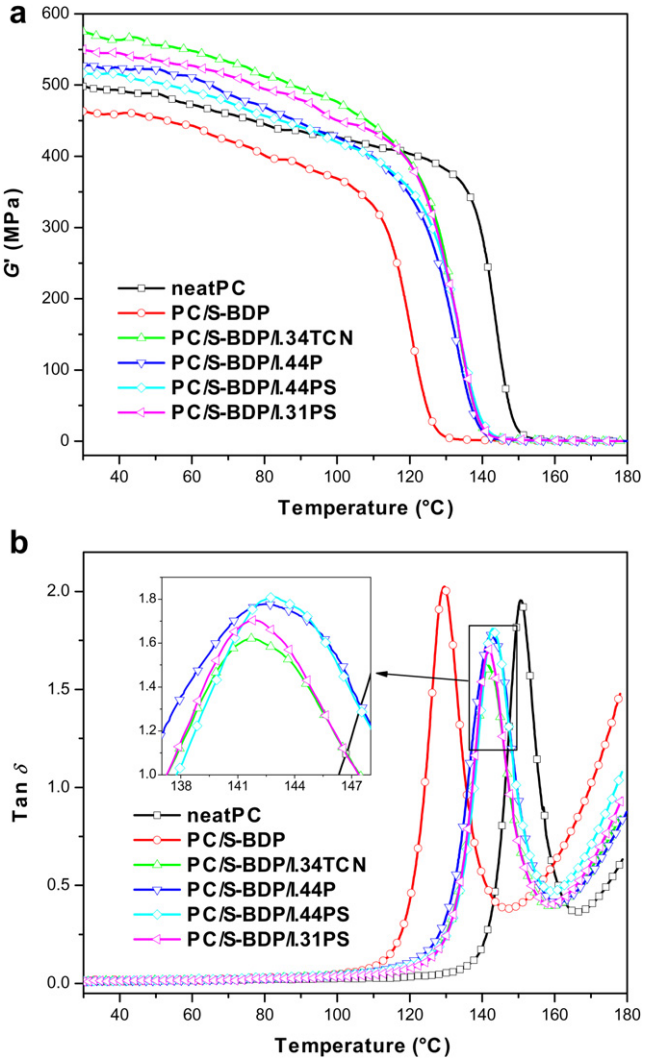

Fig. 7. (a) Storage modulus and (b) loss factor spectra of neat PC, PC/S-BDP and the nanocomposites.

It is intuitive to believe that the more chains of the matrix intercalate into the clay galleries, the more segmental motions would be constrained by the clay platelets and further lead to an enhanced thermal stability. The enhanced thermal stability is usually associated with a better flame retardancy. However, the order of the LOI values of the nanocomposites is PC/S-BDP/I.44PS > PC/S-BDP/I.31PS ≥ PC/S-BDP/I.44P > PC/S-BDP/I.34TCN, which is clearly not coherent with the trend of Δd. PC molecule is quite sensitive to water and hydroxyl groups since even a small amount of water or hydroxyl groups would initiate a massive hydrolysis or alcoholysis of the carbonate linkages [37]. The hydroxyl moieties from the modifiers of I.34TCN already bear severe risks of decomposing the matrix even during melt extrusion or injection, not to mention the risks during burning upon flame. Considering this fact, it may understand why PC/S-BDP/I.34TCN manifests the greatest intercalation of the matrix while the worst thermal stability with the lowest amount of char residue left at

Table 5
Detailed data from tensile tests and DMA.

Sample	Tensile strength (MPa)	Young's modulus (GPa)	Elongation at break (%)	G' at 30 °C (MPa)	G' at 100 °C (MPa)	T_g determined by DMA (°C)[a]
Neat PC	60.8 ± 0.5	1.91 ± 0.04	86.3 ± 12.2	498.2	426.8	150
PC/S-BDP	61.1 ± 0.8	1.80 ± 0.09	62.2 ± 10.4	463.2	368.6	130
PC/S-BDP/I.34TCN	69.7 ± 1.0	2.28 ± 0.11	15.5 ± 5.6	574.8	476.4	142
PC/S-BDP/I.44P	66.3 ± 0.8	2.08 ± 0.10	28.5 ± 8.3	527.4	427.2	142
PC/S-BDP/I.44PS	65.8 ± 0.5	2.03 ± 0.08	29.8 ± 10.1	516.7	419.8	143
PC/S-BDP/I.31PS	67.1 ± 0.7	2.17 ± 0.09	25.7 ± 7.9	549.9	450.4	142

[a] T_g determined by DMA is obtained by the temperature at the maximum value of the peak of tan δ.

800 °C. Silicon-containing compounds are considered to be flame retardants for PC [38], the extra silane coupling agent used in modification of I.44PS and I.31PS would obviously affect the thermal stability and flame retardancy of the nanocomposites. Comparing I.44P with I.44PS, they have been modified with the same type of quaternary ammonium except I.44PS has been further modified with the silane coupling agent. On one hand, PC/S-BDP/I.44PS displays a lower $T_{-5\%}$ and T_{max} than PC/S-BDP/I.44P because of the relatively worse thermal stability of the silane; on the other hand, PC/S-BDP/I.44PS demonstrates a higher LOI value since the silane could participate the char formation of the matrix upon heat to produce a more stable silicon-containing carbonaceous substance on the matrix surface [38]. A thermoplastic would melt upon heat, thus the morphology of organoclays in the thermoplastic nanocomposite during combustion could not be the same as it is under the ambient temperature. Therefore generally speaking, thermal stability and flame retardancy of nanocomposites are more strongly related the nature of chemical structures of the modifiers used for clay organic modifications than the morphology of nanocomposites revealed at the ambient temperature.

It has been reported that variations of T_g within the nanocomposites are explained by two dynamic behaviours. An increased T_g suggests a slower relaxation dynamic possibly caused by large interparticle spacings and strong polymer–nanoparticle interactions, while a decreased T_g reveals a faster relaxation dynamic possibly caused by constrained chain segments in small interparticle spacings or the plasticizing effect of the clay modifiers [14,15,39]. In our case, the shifts of T_g seem to be the competition results of the above factors. All the organoclays used here have strong interactions with the matrix to increase the T_g, especially in the I.34TCN containing nanocomposite as the modifiers bearing hydroxyl moieties. The I.44P containing nanocomposite exhibits the lowest T_g due to both weaker interactions of matrix–organoclay and a lower Δd (which implies a smaller interparticle spacing).

Regarding the thermodynamics of the nanocomposites, it was suggested that the value of heat capacity (C_P) is proportional to the parameter of internal degree of the molecular segmental motions [32,40]. Thus, the normalized change of heat capacity (ΔC_P) during glass transition of the samples, which strongly depends on the clay dispersion and the polymer concentration or the clay concentration [41], can be used for analyzing the change of the confinement of the polymer molecular segmental motions by the clay platelets. The result of ΔC_P at T_g obtained by DSC is listed in Table 4. Zhang et al. found that ΔC_P at T_g of intercalated nanocomposites decreased monotonically with the increasing clay contents [32]. In our case, the values of ΔC_P of the nanocomposites are all reduced than those of neat PC and PC/S-BDP, indicating that the molecular segmental motions of nanocomposites are constrained by clay platelets. Moreover, the order of the ΔC_P of the nanocomposites is PC/S-BDP/I.44PS > PC/S-BDP/I.44P > PC/S-BDP/I.31PS > PC/S-BDP/I.34TCN. ΔC_P at T_g is strongly related to the nanocomposite morphology, thereby it is charted versus the other parameter reflecting the clay distribution, changes of d_{001} spacing between filled and unfilled organoclays (Δd), in Fig. 8. It is unambiguous that ΔC_P decreases with increasing Δd. The higher Δd reveals more polymer chain segments intercalated into clay platelets hence more amount of segmental motions is constrained, leading to a decreased ΔC_P.

Both the tensile and DMA results show that with only 2 wt. % organoclay, despite the modifier used, modulus would be prominently increased. Trends of tensile strength, Young's modulus and storage modulus are all coincident with that of Δd. It establishes that morphology of the nanocomposites is one of the factors affecting the mechanical properties. Mechanical reinforcement of polymer composites is explained by the constraint or confinement of polymer chains to the filler surface. Since the organoclays display large surface areas and aspect ratios, the reinforcement would be much more efficient than conventional micro-fillers. The enhancement of the modulus can be predicted by a mixing law [4,32]. It assumes that in a nanocomposite, the region of unconstrained polymer chains would exhibit the same modulus as in the unfilled matrix, whereas region of constrained chains by organoclays would exhibit a higher modulus. Consequently, the modulus of the nanocomposite can be calculated as a mixer of the unconstrained and constrained regions. It can be expressed as

$$G'_n = G'_m(1 - C) + G'_c C \quad (1)$$

where C is the volume fraction of the constrained region, while G'_n, G'_m and G'_c are storage modulus of the nanocomposite, the unfilled matrix and the constrained region below T_g, respectively. Therefore, the storage modulus of the constrained region can be expressed by rearranging equation (1) to be

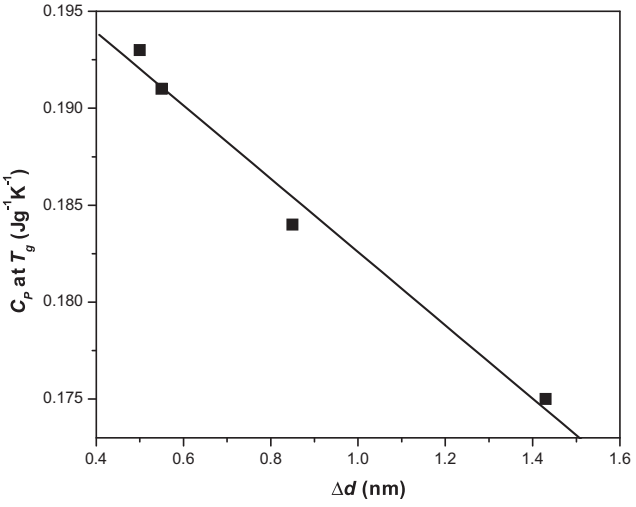

Fig. 8. The relationship between polymer intercalation (suggested by Δd_{001}) and normalized change in heat capacity at glass transition (ΔC_P at T_g).

$$G'_c = \frac{1}{C}(G'_n - G'_m) + G'_m \quad (2)$$

Meanwhile, the height or the area of the loss factor (tan δ) reflects the volume fraction of the constrained region [4,32,42], and the volume fraction of the constrained region can be calculated by the loss factor. In amorphous polymer system, their relationship can be established as

$$C = \left(1 - \frac{W_n}{W_m}\right) \times 100\% \quad (3)$$

$$W = \frac{\pi \tan\ \delta}{\pi \tan\ \delta + 1} \quad (4)$$

where W is the energy loss fraction, and the subscripts n and m refer to nanocomposites and unfilled matrix. Employing equations (2)–(4) and the data from DMA, the volume fractions and storage moduli of the constrained regions of all the four nanocomposites studied in this research can be calculated. These results are listed in Table 6. Note that these nanocomposites are all filled with 6 wt. % S-BDP and 0.4 wt. % PTFE, thus the value of G'_m and W_m is based on PC/S-BDP rather than neat PC. From the results listed in Table 6, one can find that the order of the volume fraction of the constrained region among the nanocomposites is PC/S-BDP/I.34TCN > PC/S-BDP/I.31PS > PC/S-BDP/I.44P > PC/S-BDP/I.44PS, which is the same trend of the Δd. More intercalations may lead to a larger volume fraction of the constrained region, that is to say the volume fraction of the constrained region is associated with the morphology of the nanocomposite. Concerning the storage moduli of the constrained region, the four nanocomposites show almost no differences at the ambient temperature (30 °C). However, the situation varies at a higher temperature (100 °C). Despite there may be some other factors such as the molecular weight of the matrix or the aspect ratio of the dispersed clays, different affinities between the matrix and the organoclays must be responsible for the different storage moduli of the constrained region at the higher temperature. The effect of the affinity could not be clearly revealed at a lower temperature due to the motions of both polymer chains and organoclays are "frozen"; however, the motions can be more "activated" at the higher temperature thus the different interactions between the matrix and organoclays become more significant. The modifier of I.34TCN bears hydroxyl moieties which can strongly interact with the matrix by hydrogen bonding; therefore, the storage modulus of the constrained region of PC/S-BDP/I.34TCN exhibits the highest value. When additionally modified with a silane, the clays would be expected to be more hydrophobic thereby more compatible with the matrix. Hence, the storage modulus of the constrained region of PC/S-BDP/I.44P is lower than that of PC/S-BDP/I.44PS and PC/S-BDP/I.31PS. Also, the increased value of PC/S-BDP/I.44PS compared to PC/S-BDP/I.31PS reveals that the modifier bearing two long alkyl tails has stronger interactions with the matrix than the one bearing a single long alkyl tail. To sum up, the mechanical reinforcement of the nanocomposites is basically affected by both the morphology and the affinity of the organoclays with the matrix.

Table 6
The volume fractions and storage moduli of the constrained regions in the nanocomposites.

Sample	C (vol. %)	G'_c at 30 °C (GPa)	G'_c at 100 °C (GPa)
PC/S-BDP/I.34TCN	3.24	3.92	3.70
PC/S-BDP/I.44P	1.85	3.93	3.53
PC/S-BDP/I.44PS	1.55	3.91	3.67
PC/S-BDP/I.31PS	2.51	3.92	3.63

5. Conclusions

Flame retarded polycarbonate nanocomposites have been produced by melt blending bisphenol A PC with solid BDP and a series of organoclays modified with different organic modifiers. Keeping the total loading of S-BDP and organoclay to be 8 wt. % as well as PTFE to be 0.4 wt. %, the best flame retardancy can be always achieved in the sample filled with 2 wt. % organoclay and 6 wt. % S-BDP whichever type of organoclay is used. Although the morphologies of the nanocomposites are all intercalated-exfoliated, a slight difference in the intercalation magnitude could be discerned by the varied increments of the clay basal spacing. Flammability of the nanocomposites can be associated with the corresponding thermal stability rather than the morphology. The unfortunately reduced T_g due to the plasticizing effect of S-BDP can be compensated by organoclays. A mixing law has been adopted to study the reinforcement, and it shows that the mechanical properties are affected by both the morphology and affinity of the organoclays with the matrix. The modifier bearing hydroxyl moieties has stronger interactions with the matrix, thus the corresponding nanocomposite exhibits a better intercalated morphology, higher T_g, improved strength and modulus; on the other hand, the hydroxyl moieties would promote degradation of the matrix, thereby the nanocomposite shows a worse thermal stability and flame retardancy. Organoclays additionally modified with a silane are more compatible with the matrix, however the steric effect of the silane would hinder the intercalation of the polymer chains resulting a smaller strength and modulus of the nanocomposites. Nevertheless, flammability of the nanocomposite is further reduced because of the flame retardant effect of the silane. Compared to the modifier bearing a single long alkyl tail, the one bearing two tails also shows stronger affinity with the matrix but a less intercalated morphology due to the steric effect.

Effects of the organoclay modifiers on the flammability, thermal and mechanical properties of the nanocomposites have been established by comprehensive investigations. A trade-off choice could be made during practical applications based on this research.

References

[1] Innes J, Innes A. Flame retardants for polycarbonate – new and classical solutions. Plast Addit Compound 2006;8:26–9.
[2] Levchik SV, Weil ED. Overview of recent developments in the flame retardancy of polycarbonates. Polym Int 2005;54:981–98.
[3] Levchik SV, Bright DA, Moy P, Dashevsky S. New developments in fire retardant non-halogen aromatic phosphates. J Vinyl Addit Technol 2000;6:123–8.
[4] Kojima Y, Usuki A, Kawasumi M, Okada A, Fukushima Y, Kurauchi T, et al. Mechanical-properties of nylon 6-clay hybrid. J Mater Res 1993;8:1185–9.
[5] Usuki A, Kojima Y, Kawasumi M, Okada A, Fukushima Y, Kurauchi T, et al. Synthesis of nylon 6-clay hybrid. J Mater Res 1993;8:1179–84.
[6] Kojima Y, Usuki A, Kawasumi M, Okada A, Kurauchi T, Kamigaito O. Synthesis of nylon-6-clay hybrid by montmorillonite intercalated with epsilon-caprolactam. J Polym Sci Part A-Polym Chem 1993;31:983–6.
[7] Morgan AB. Flame retarded polymer layered silicate nanocomposites: a review of commercial and open literature systems. Polym Adv Technol 2006;17:206–17.
[8] Okada A, Usuki A. Twenty years of polymer–clay nanocomposites. Macromol Mater Eng 2006;291:1449–76.
[9] Chen B, Evans JRG, Greenwell HC, Boulet P, Coveney PV, Bowden AA, et al. A critical appraisal of polymer–clay nanocomposites. Chem Soc Rev 2008;37:568–94.
[10] Paul DR, Robeson LM. Polymer nanotechnology: nanocomposites. Polymer 2008;49:3187–204.
[11] Pavlidou S, Papaspyrides CD. A review on polymer–layered silicate nanocomposites. Prog Polym Sci 2008;33:1119–98.
[12] Kiliaris P, Papaspyrides CD. Polymer/layered silicate (clay) nanocomposites: an overview of flame retardancy. Prog Polym Sci 2010;35:902–58.
[13] Dai XH, Xu J, Guo XL, Lu YL, Shen DY, Zhao N, et al. Study on structure and orientation action of polyurethane nanocomposites. Macromolecules 2004;37:5615–23.
[14] Park J, Jana SC. Adverse effects of thermal dissociation of alkyl ammonium ions on nanoclay exfoliation in epoxy-clay systems. Polymer 2004;45:7673–9.

[15] Vaia RA, Sauer BB, Tse OK, Giannelis EP. Relaxations of confined chains in polymer nanocomposites: glass transition properties of poly(ethylene oxide) intercalated in montmorillonite. J Polym Sci Part B-Polym Phys 1997;35:59–67.
[16] Huang XY, Lewis S, Brittain WJ, Vaia RA. Synthesis of polycarbonate-layered silicate nanocomposites via cyclic oligomers. Macromolecules 2000;33:2000–4.
[17] Lee KM, Han CD. Effect of hydrogen bonding on the rheology of polycarbonate/organoclay nanocomposites. Polymer 2003;44:4573–88.
[18] Mitsunaga M, Ito Y, Ray SS, Okamoto M, Hironaka K. Intercalated polycarbonate/clay nanocomposites: nanostructure control and foam processing. Macromol Mater Eng 2003;288:543–8.
[19] Yoon PJ, Hunter DL, Paul DR. Polycarbonate nanocomposites. Part 1. Effect of organoclay structure on morphology and properties. Polymer 2003;44:5323–39.
[20] Hsieh AJ, Moy P, Beyer FL, Madison P, Napadensky E, Ren JX, et al. Mechanical response and rheological properties of polycarbonate layered-silicate nanocomposites. Polym Eng Sci 2004;44:825–37.
[21] Wu DF, Wu LF, Zhang M, Wu L. Effect of epoxy resin on rheology of polycarbonate/clay nanocomposites. Eur Polym J 2007;43:1635–44.
[22] Carrion FJ, Arribas A, Bermudez MD, Guillamon A. Physical and tribological properties of a new polycarbonate–organoclay nanocomposite. Eur Polym J 2008;44:968–77.
[23] Chow WS, Neoh SS. Dynamic mechanical, thermal, and morphological properties of silane-treated montmorillonite reinforced polycarbonate nanocomposites. J Appl Polym Sci 2009;114:3967–75.
[24] Cui LL, Bara JE, Brun Y, Yoo Y, Yoon PJ, Paul DR. Polyamide- and polycarbonate-based nanocomposites prepared from thermally stable imidazolium organoclay. Polymer 2009;50:2492–502.
[25] Nevalainen K, Vuorinen J, Villman V, Suihkonen R, Jarvela P, Sundelin J, et al. Characterization of twin-screw-extruder-compounded polycarbonate nanoclay composites. Polym Eng Sci 2009;49:631–40.
[26] Nayak SK, Mohanty S, Samal SK. Mechanical and thermal properties enhancement of polycarbonate nanocomposites prepared by melt compounding. J Appl Polym Sci 2010;117:2101–12.
[27] Rama MS, Swaminathan S. Polycarbonate/clay nanocomposites via in situ melt polycondensation. Ind Eng Chem Res 2010;49:2217–27.
[28] Feng J, Hao JW, Du JX, Yang RJ. Flame retardancy and thermal properties of solid bisphenol A bis(diphenyl phosphate) combined with montmorillonite in polycarbonate. Polym Degrad Stab 2010;95:2041–8.
[29] Feng J, Hao JW, Du JX, Yang RJ. Using TGA/FTIR TGA/MS and cone calorimetry to understand thermal degradation and flame retardancy mechanism of polycarbonate filled with solid bisphenol A bis(diphenyl phosphate) and montmorillonite. Polym Degrad Stab, submitted for publication.
[30] Qin HL, Zhang SM, Zhao CG, Hu GJ, Yang MS. Flame retardant mechanism of polymer/clay nanocomposites based on polypropylene. Polymer 2005;46:8386–95.
[31] http://www.bayermaterialscience.com/internet/global_portal_cms.nsf/id/EN_Informationsmaterial_PCS [last accessed in August, 2011].
[32] Zhang XG, Loo LS. Study of glass transition and reinforcement mechanism in polymer/layered silicate nanocomposites. Macromolecules 2009;42:5196–207.
[33] Awad WH, Beyer G, Benderly D, Ijdo WL, Songtipya P, Jimenez-Gasco MD, et al. Material properties of nanoclay PVC composites. Polymer 2009;50:1857–67.
[34] Aranda P, Ruizhitzky E. Poly(ethylene oxide)-silicate intercalation materials. Chem Mater 1992;4:1395–403.
[35] Chen BQ, Evans JRG. Poly(epsilon-caprolactone)-clay nanocomposites: structure and mechanical properties. Macromolecules 2006;39:747–54.
[36] Triantafyllidis KS, LeBaron PC, Pinnavaia TJ. Thermoset epoxy-clay nanocomposites: the dual role of alpha, omega-diamines as clay surface modifiers and polymer curing agents. J Solid State Chem 2002;167:354–62.
[37] Jang BN, Wilkie CA. A TGA/FTIR and mass spectral study on the thermal degradation of bisphenol A polycarbonate. Polym Degrad Stab 2004;86:419–30.
[38] Masatoshi I, Serizawa S. Silicone derivatives as new flame retardants for aromatic thermoplastics used in electronic devices. Polym Adv Technol 1998;9:593–600.
[39] Khan AN, Hong PD, Chuang WT, Shih KS. Effect of uniaxial drawing on the structure and glass transition behaviour of poly(trimethylene 2,6-naphthalate)/layered clay nanocomposites. Polymer 2009;50:6287–96.
[40] Vyazovkin S, Dranca I. A DSC study of alpha and beta-relaxations in a PS-clay system. J Phys Chem B 2004;108:11981–7.
[41] Li YQ, Ishida H. A study of morphology and intercalation kinetics of polystyrene–organoclay nanocomposites. Macromolecules 2005;38:6513–9.
[42] An L, Pan YZ, Shen XW, Lu HB, Yang YL. Rod-like attapulgite/polyimide nanocomposites with simultaneously improved strength, toughness, thermal stability and related mechanisms. J Mater Chem 2008;18:4928–41.